Supplementary information

Unveiling adsorption tendency of film-forming additives to enable the fast-charging hard carbon anode with regulated Li plating

Yongteng Dong[a], Yuanmao Chen[a], Xinyang Yue[a, *], Zheng Liang[a, *]

[a] Frontiers Science Center for Transformative Molecules, School of Chemistry and Chemical Engineering, Shanghai Jiao Tong University, Shanghai 200240, China.

* E-mail address: xinyangyue@sjtu.edu.cn; liangzheng06@sjtu.edu.cn

Materials and Methods

Materials. Battery-grade Li salt, solvent, diluent, and additives, including lithium bis(fluorosulfonyl)imide (LiFSI), lithium hexafluorophosphate (LiPF$_6$), dimethyl carbonate (DMC), 1,1,2,2–tetrafluoroethyl–2,2,3,3–tetrafluoropropyl ether (HFE), ethylene carbonate (EC) and fluoroethylene carbonate (FEC) were purchased from DoDoChem Co., Ltd. Li metal chips in diameter of 15.6 mm with a thickness of 450 μm were purchased from China Energy Lithium Co., Ltd. The Kuraray hard carbon (HC, anode) powders were purchased from Foshan Porous Carbon Tech Co., Ltd. LiFePO$_4$ (LFP, cathode) powders were purchased from Hefei Kejing Materials Technology Co., Ltd. All of the materials in the work were used as received unless otherwise stated.

Electrolyte and electrode preparation. Electrochemical experiments were performed using CR2032-type coin cells and Celgard 2400 separators. All of the cells were assembled in an Ar-filled glove box (< 0.1 ppm O$_2$, < 0.1 ppm H$_2$O). Hard carbon electrodes with the areal capacity of 0.9 and 1.5 mAh cm^{-2} were prepared by dissolution of 90 wt.% HC, 5 wt.% carbon black, 3 wt.% carboxymethyl cellulose (CMC), and 2 wt.% styrene-butadiene rubber binder (SBR) in deionized water. The obtained slurry was coated onto Cu foil for the HC electrode fabrication. Li metal chips with a diameter of 15.6 mm served as counter electrodes. For full-cell measurements, the LFP electrode was prepared by dissolving 92 wt.% LFP powders, 5 wt.% carbon black, and 3 wt.% polyvinylidene fluoride (PVDF) binder into N–methyl–2–pyrrolidone (NMP) solvent. For three-electrode cell measurements, a thin Li metal chip as a reference electrode was placed between the LFP cathode and the HC anode. The self-made pouch cells were prepared using a single-layer LFP cathode and HC anode in the dimension of 4.1 cm × 5.1 cm. The conventional concentration electrolyte (CCE) was prepared by dissolving 1.0 M LiPF$_6$ into EC: DMC (1:1 in volume). The baseline local high concentration electrolyte (LHCE) was made by dissolving 1.4 M LiFSI in DMC: HFE (25: 40 in volume). 1.0 vol.% film-forming additive (EC or FEC) was added into LHCE depending on electrolyte compositions investigated in the study. 40 μL electrolyte was added in each coin cell for testing.

Materials Characterization. The impedance before and after Li plating was analyzed using Electrochemical Impedance Spectroscopy (EIS; Bio-logic VMP300 workstation) with a frequency range from 100 kHz to 0.1 Hz. Time of flight secondary ion mass spectrometry (TOF-SIMS) (GAIA3) was applied to monitor elemental Li distribution on the HC anode surface. The morphology was characterized by scanning electron microscopy (SEM) (JSM 7401F, JEOL Ltd., Japan) and transmission electron microscope (TEM) (Talos F200X G2). The Young's modulus of samples was tested by the tapping mode of the atomic force microscopy (AFM) (MFP-3D) in the Ar atmosphere. The argon ion etching-assisted X-ray photoelectron spectroscopy (XPS) was collected using a Kratos AXIS UltraDLD X-ray photoelectron spectrometer excited by monochromatic Al (1486.7 eV, 240 W) source. Before each characterization test, HC samples were rinsed by DMC for three times to remove residual Li salts and dried under vacuum protection. The Li^+ transference number (t_{Li+}) was determined at 25 °C by combining EIS and chronoamperometry with a polarization voltage (ΔV) of 10 mV using Li‖Li symmetrical cells. The t_{Li+} was calculated by the following equation (S1):

$$t_{Li^+} = \frac{I_s(\Delta V - I_0 R_0)}{I_0(\Delta V - I_s R_s)}$$

(Equation S1)

Io and *Is* are the initial and steady currents during polarization, respectively. *Ro* and *Rs* are the initial and steady surface impedance of the measured cell, respectively.

Computational and density functional theory (DFT) calculations. Quantum chemistry calculations were first performed to optimize molecular geometries of DMC, EC, FEC, and HFE solvent molecules using the Gaussian 16 package at B3LYP/6-311 + G(d,p) level of theory[1]. The atomic partial charges on these molecules were calculated using the ChelpG method at the same level of theory (the B3LYP hybrid functional and the 6-311 + G(d,p) basis set). The atomistic force field parameters for all ions and solvent molecules are described by the AMBER format and are taken from a previous work[2]. The cross-interaction parameters between different atom types are obtained from the Lorentz-Berthelot combination rule.

Three modelling systems were constructed. All atomistic simulations were performed using GROMACS package with cubic periodic boundary conditions[3]. The equations for the motion of all atoms were integrated using a classic Verlet leapfrog integration algorithm with

a time step of 1.0 fs. A cutoff radius of 1.6 nm was set for short-range van der Waals interactions and real-space electrostatic interactions. The particle-mesh Ewald (PME) summation method with an interpolation order of 5 and a Fourier grid spacing of 0.20 nm was employed to handle long range electrostatic interactions in reciprocal space. All simulation systems were first energetically minimized using a steepest descent algorithm, and thereafter annealed gradually from 600 K to room temperature (300 K) within 10 ns. All annealed simulation systems were equilibrated in an isothermal-isobaric (NPT) ensemble for 20 ns of physical time maintained using a Nosé-Hoover thermostat and a Parrinello-Rahman barostat with time coupling constants of 0.4 and 0.2 ps, respectively, to control the temperature at 300 K and the pressure at 1 atm. Atomistic simulations were further performed in a canonical ensemble (NVT) for 40 ns, and simulation trajectories were recorded at an interval of 100 fs for further structural and dynamical analysis.

The stepwise lithiation process was carried out using COMSOL Multiphysics to investigate the Li plating morphology on the anode based on a two-dimensional (2D) transient model of electrodeposition.[4-6] The 2D model consisted of an electrolyte with a thickness of 5 μm and a vertically aligned micro sheet sphere with a height of 15 μm. The width of the micro sheet sphere was set to be 10 μm, and the distance between two adjacent nanosheets was 4 μm. The concentration of Li ions was set to be 1.4 mol L^{-1} and the current density in the bulk electrolyte was 1 mA cm^{-2}.

The adsorption energies of EC and FEC molecules, and FSI anion on the graphic layer with a single vacancy defect were calculated at the DFT level with the PBE exchange-correlation functional by the Vienna *ab initio* simulation package.[7-9] The interaction between the atomic cores and the electrons was described with the projector-augmented wave method.[10] Dispersion interactions were described using the optimized optPBE-vdw functional with a cutoff energy of 420 eV.[11]

The DFT calculations of HC slabs were performed using an 8 × 8 supercell and a 2 × 2 × 1 Γ-centered Monkhorst-Pack k-point grid. Two graphene layers were selected to model the adsorptions of EC/FEC molecules, FSI anion, and EC-FSI/FEC-FSI structures on HC slabs, and the bottom layer was fixed during DFT calculations.

Structure optimizations were carried out when the residual force was less than 0.02 eV Å^{-1} for each atom, and the total energy is converged within 10^{-4} eV. The adsorption energy (E_{ads}) was obtained by the equation below.

$$\Delta E_{ads} = E_{slab+adsorbate} - E_{slab} - E_{adsorbate} \qquad \text{(Equation S2)}$$

where $E_{slab+adsorbate}$ and E_{slab} are the total electronic energies of the HC surface slab with and without the adsorbate, respectively. $E_{adsorbate}$ is the electronic energy of the adsorbate in the gas phase, which was calculated with a 12.0 Å × 12.0 Å × 12.0 Å unit cell at the gamma point.

SI Figures and Tables
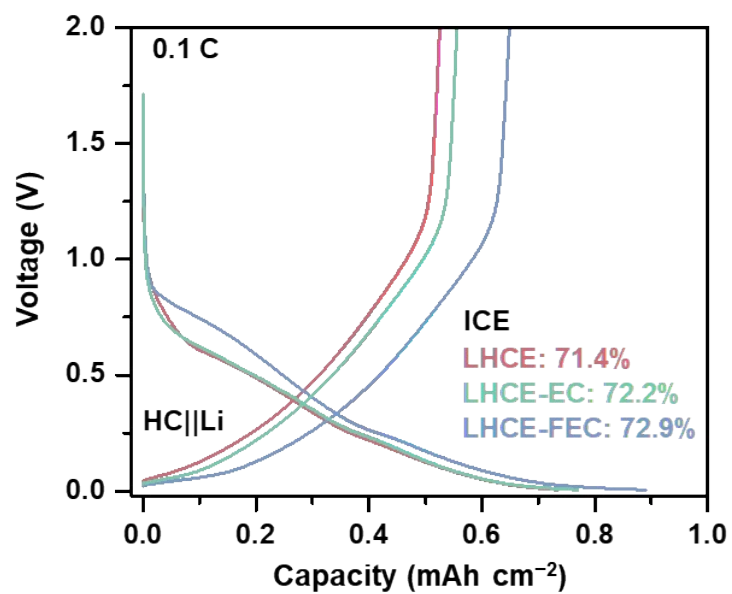
Figure S1. Voltage curves of the HC anode using LHCE, LHCE-EC, and LHCE-FEC at the initial cycle under 0.1 C. Voltage range: 0.005~2.0 V.
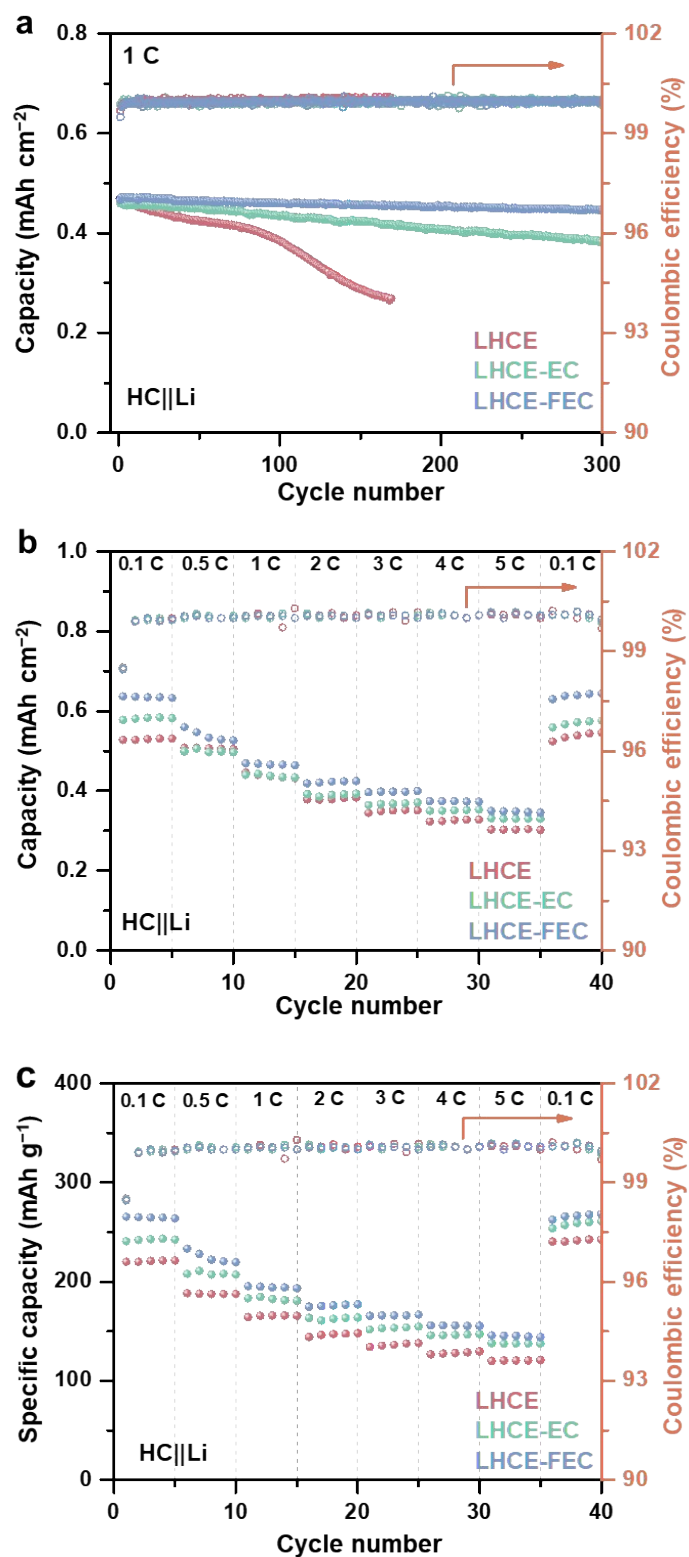
Figure S2. (a) Galvanostatic cycling of the HC anode half-cells in LHCE, LHCE-EC, and LHCE-FEC at 1 C. (b) Rate performance of the HC anode in LHCE, LHCE-EC, and LHCE-FEC at 0.1~5 C. (c) Rate performance of HC||Li half cells using LHCE, LHCE-EC, and LHCE-FEC at 0.1~5 C in specific capacity. 1 C = 0.9 mAh cm^{-2}. Voltage range: 0.005~2.0 V.
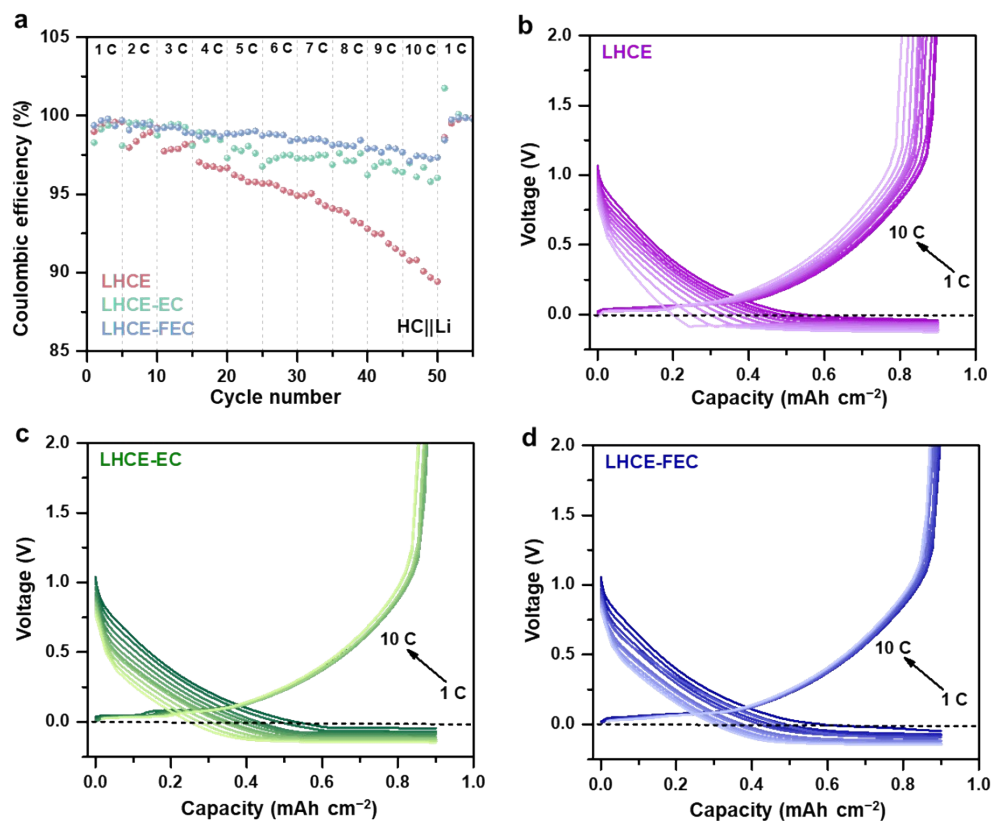
Figure S3. (a) CE of CLC rate test for half cells using LHCE, LHCE-EC, and LHCE-FEC at 1~10 C. (b) Voltage curves of half cells in CLC rate test from 1 to 10 C in LHCE. (c) Voltage curves of half cells in CLC rate test from 1 to 10 C in LHCE-EC. (d) Voltage curves of half cells in CLC rate test from 1 to 10 C in LHCE-FEC. Cycling conditions: half cells were lithiated to 0.9 mAh cm^{-2} then de-lithiated to 2.0 V. The lithiation rate was gradually ramped up from 1 to 10 C every 5 cycles, and the de-lithiation rate remains at 1 C constantly. 1 C = 0.9 mAh cm^{-2}.
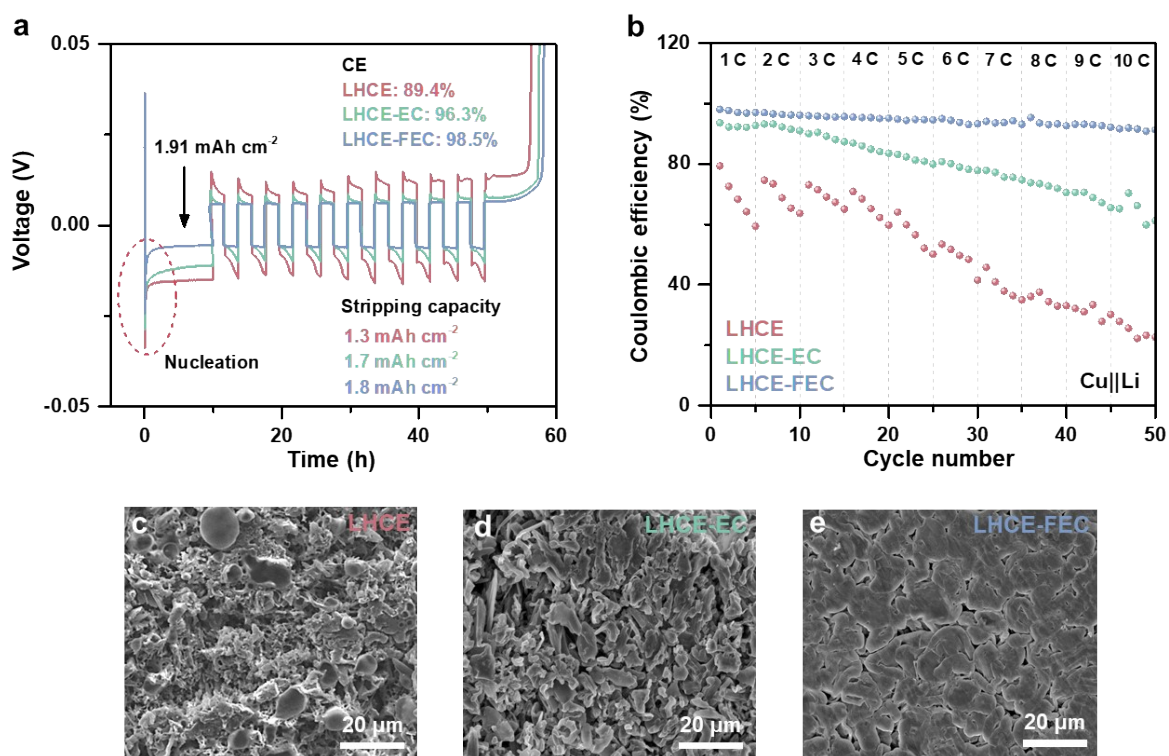
Figure S4. (a) Li deposition/stripping test of Cu‖Li cells using LHCE, LHCE-EC, and LHCE-FEC at a current density of 0.9 mA cm^{-2} with an areal capacity of 0.9 mAh cm^{-2}. (b) Rate performance of Cu‖Li cells by CLC test in LHCE, LHCE-EC, and LHCE-FEC. (c-e) SEM images of Li plating on Cu foil in LHCE, LHCE-EC, and LHCE-FEC, respectively. 1 C = 0.9 mAh cm^{-2}. Cut-off voltage: ~2.0 V.
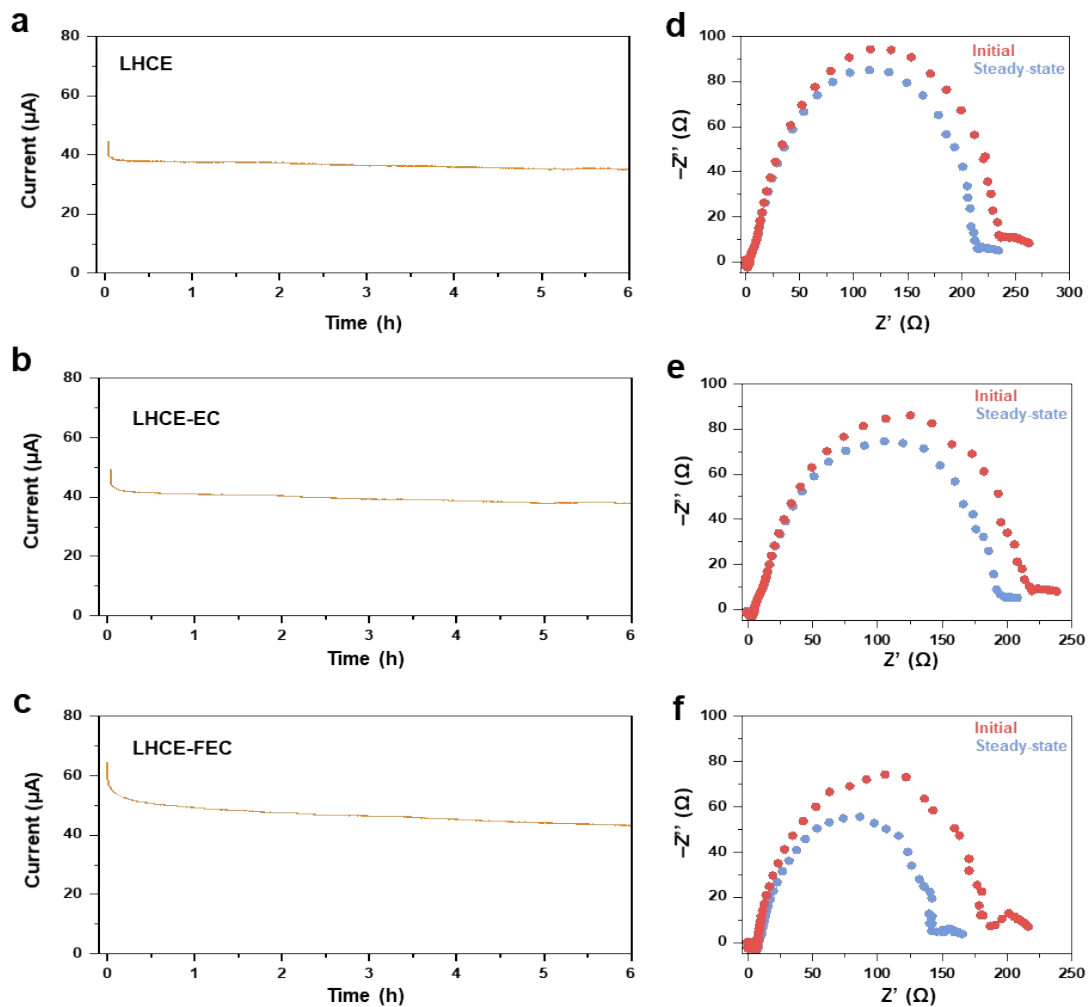
Figure S5. Potentiostatic polarization curves of Li‖Li symmetrical cells for transference number tests in (a) LHCE, (b) LHCE-EC, and (c) LHCE-FEC. Nyquist plot of the AC impedance spectra of Li‖Li symmetrical cells before (R_o) and after (R_s) potentiostatic polarization tests in (d) LHCE, (e) LHCE-EC, and (f) LHCE-FEC.
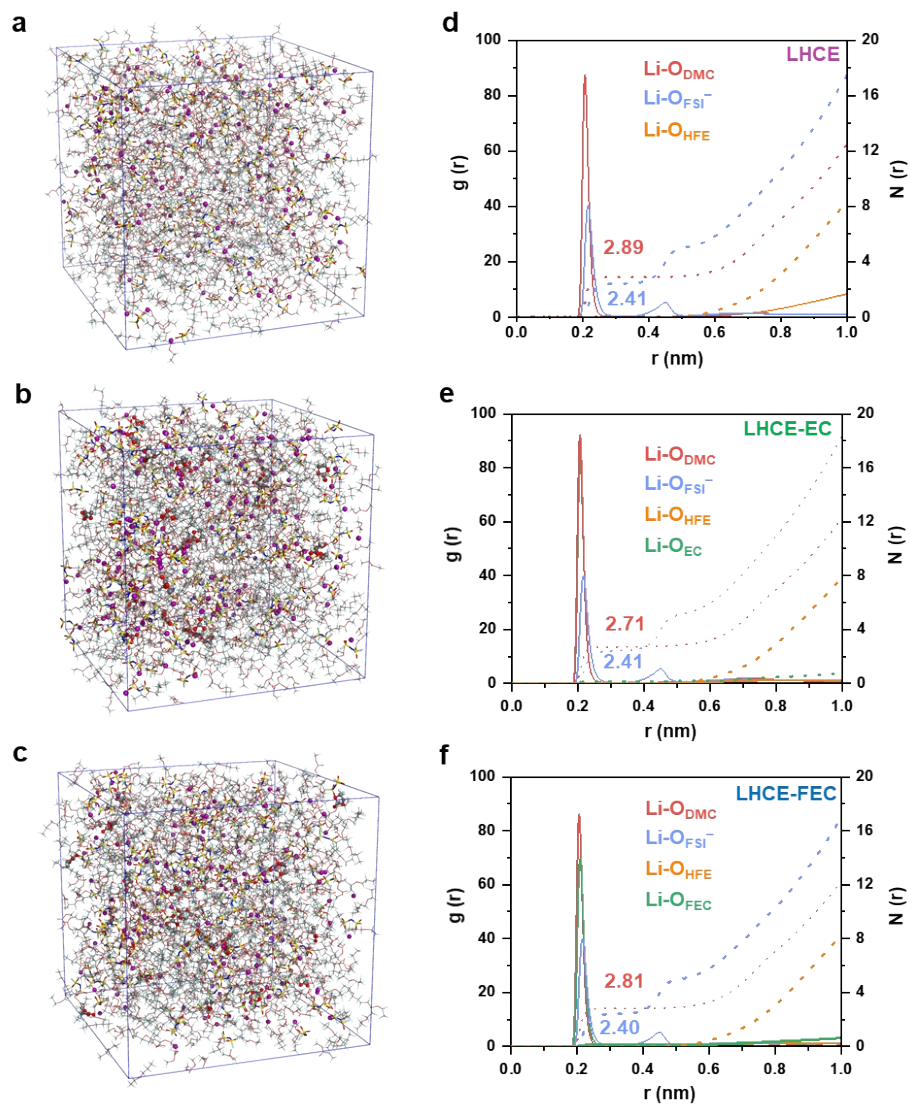
Figure S6. Snapshot of MD simulation at 30 °C with respect to (a) LHCE, (b) LHCE-EC, and (c) LHCE-FEC. Radial distribution functions of DMC oxygen, FSI⁻ oxygen, HFE oxygen, and FEC oxygen with respect to Li⁺ ion in (d) LHCE, (e) LHCE-EC, and (f) LHCE-FEC.
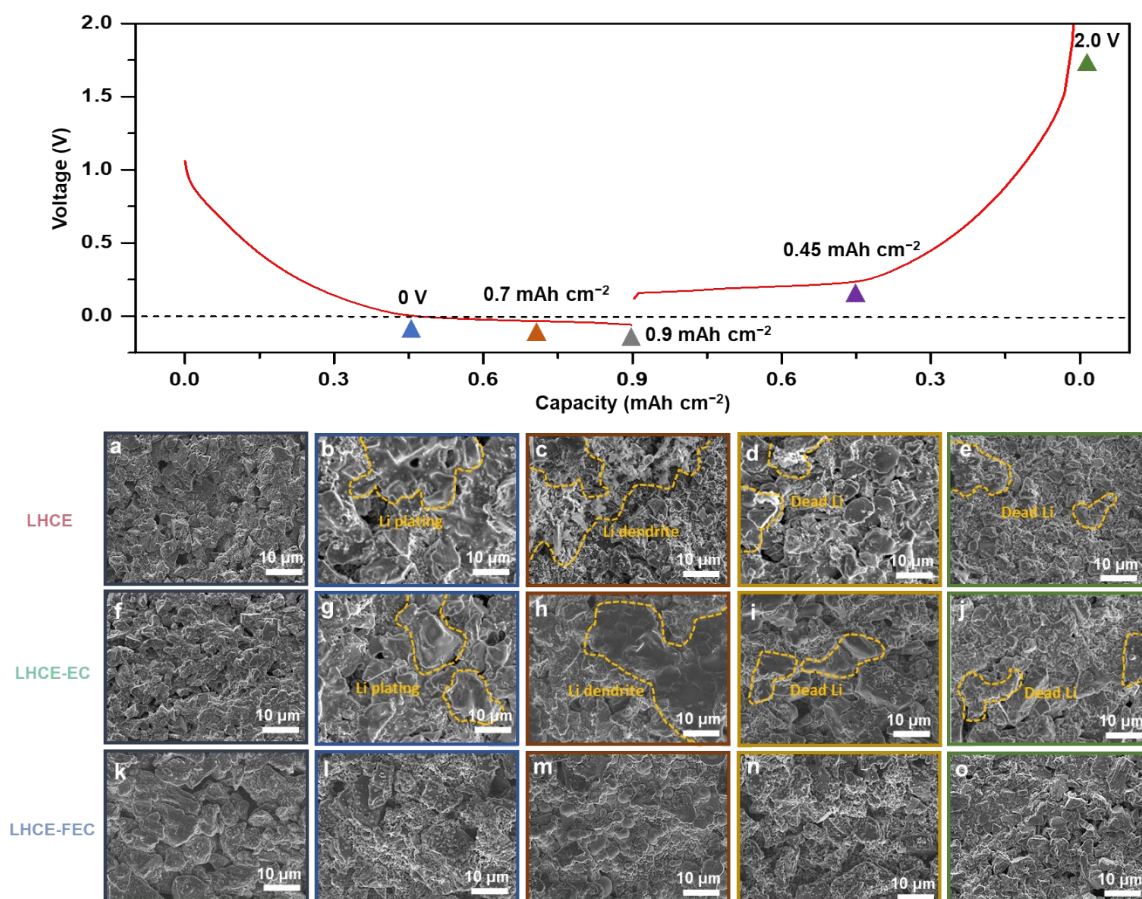
Figure S7. SEM images of CLC test using LHCE after lithiation to (a) 0 V, (b) 0.7 mAh cm^{-2}, (c) 0.9 mAh cm^{-2}, then de-lithiation to (d) 0.45 mAh cm^{-2}, and (e) 2.0 V at 1 C. SEM images of CLC test using LHCE-EC after lithiation to (f) 0 V, (g) 0.7 mAh cm^{-2}, (h) 0.9 mAh cm^{-2}, then de-lithiation to (i) 0.45 mAh cm^{-2}, and (j) 2.0 V at 1 C. SEM images of CLC test using LHCE-FEC after lithiation to (k) 0 V, (l) 0.7 mAh cm^{-2}, (m) 0.9 mAh cm^{-2}, then de-lithiation to (n) 0.45 mAh cm^{-2}, and (o) 2.0 V at 1 C. 1 C = 0.9 mAh cm^{-2}.
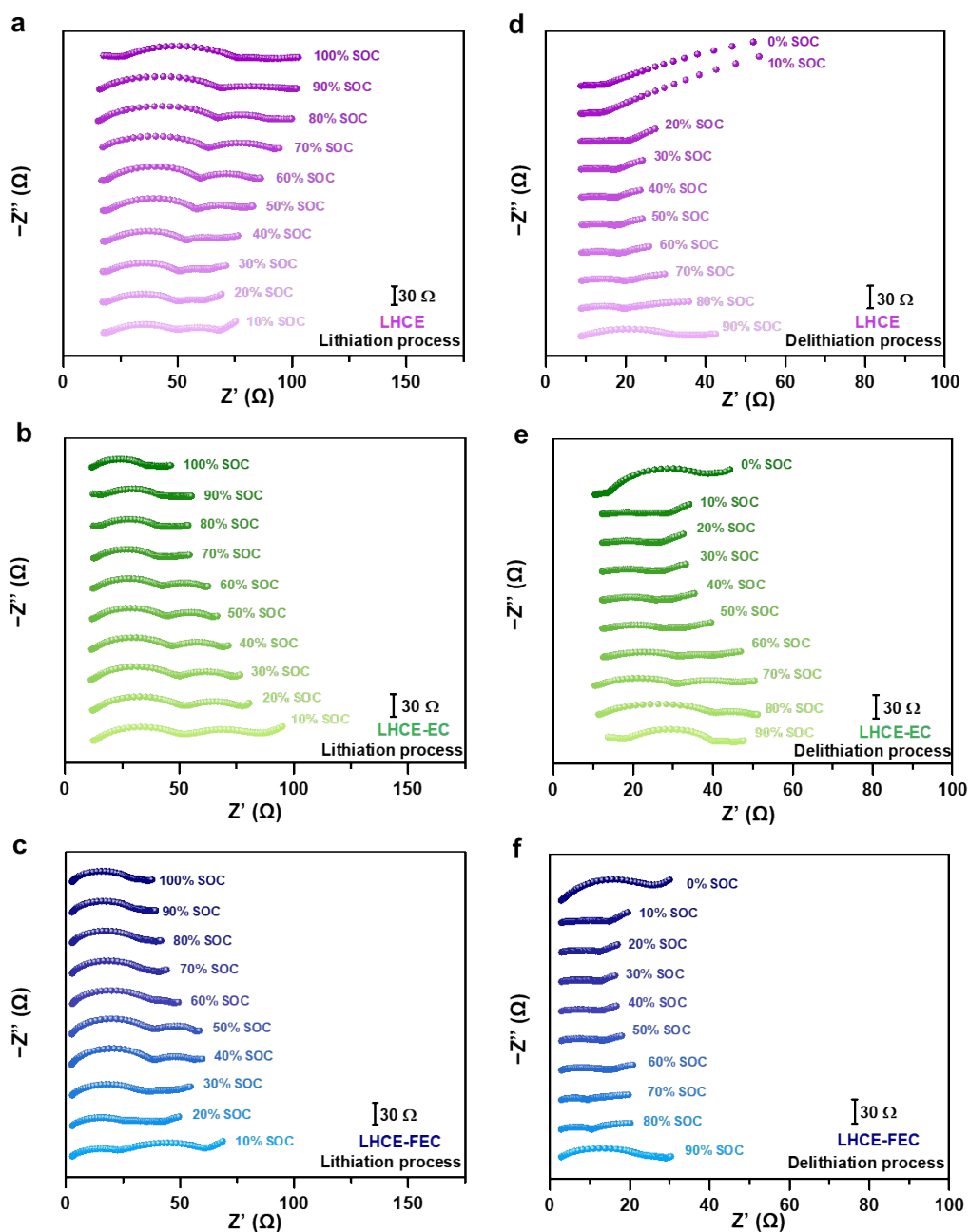
Figure S8. EIS profiles of (a) LHCE, (b) LHCE-EC and (c) LHCE-FEC half cells at the SOC from 10 to 100% during lithiation at 1 C, respectively. EIS profiles of (d) LHCE, (e) LHCE-EC and (f) LHCE-FEC half cells at the SOC from 90 to 0% during de-lithiation at 1 C, respectively. 1 C = 0.9 mAh cm^{-2}.
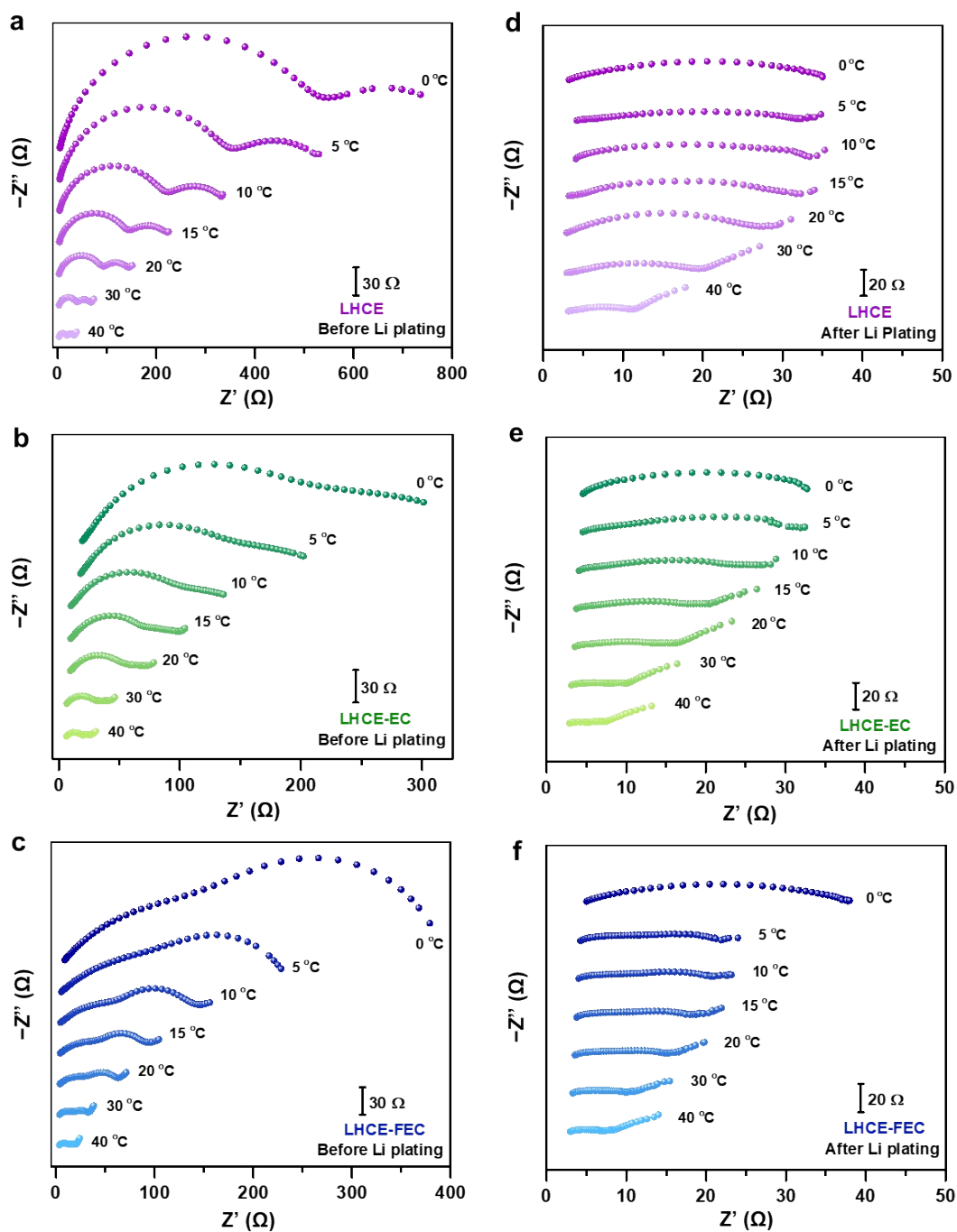
Figure S9. Temperature-dependent EIS measurements for cells containing (a) LHCE, (b) LHCE-EC, and (c) LHCE-FEC before Li plating. Temperature-dependent EIS measurements for cells containing (d) LHCE, (e) LHCE-EC and (f) LHCE-FEC after Li plating.
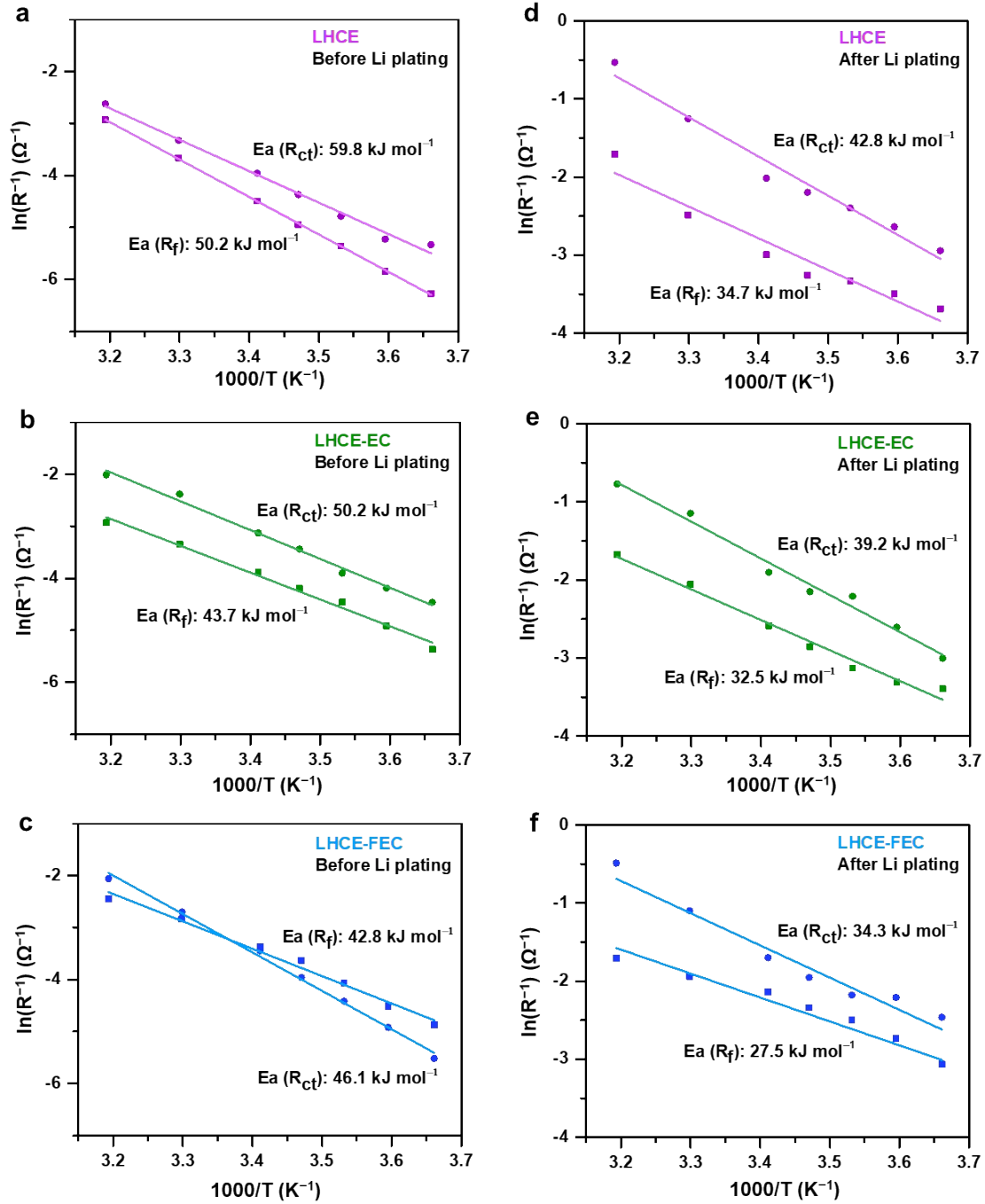
Figure S10. Arrhenius behavior of the resistance for Li-ion de-solvation and diffusion through SEI in (a) LHCE, (b) LHCE-EC, and (c) LHCE-FEC before Li plating. Arrhenius behavior of the resistance for Li-ion de-solvation and diffusion through SEI in (d) LHCE, (e) LHCE-EC, and (f) LHCE-FEC after Li plating. The E_a values can be obtained according to the equation below,

$$R^{-1} = Ae^{-\frac{E_a}{RT}}$$

(Equation S3)

where R is the molar gas constant (8.314 J mol·K^{-1}), T is the thermodynamic temperature in Kelvin scale, and A is the pre-exponential factor. Then, both charge-transfer resistance (R_{ct}) and SEI resistance (R_f) can be calculated by fitting the EIS spectra in the Arrhenius plot.
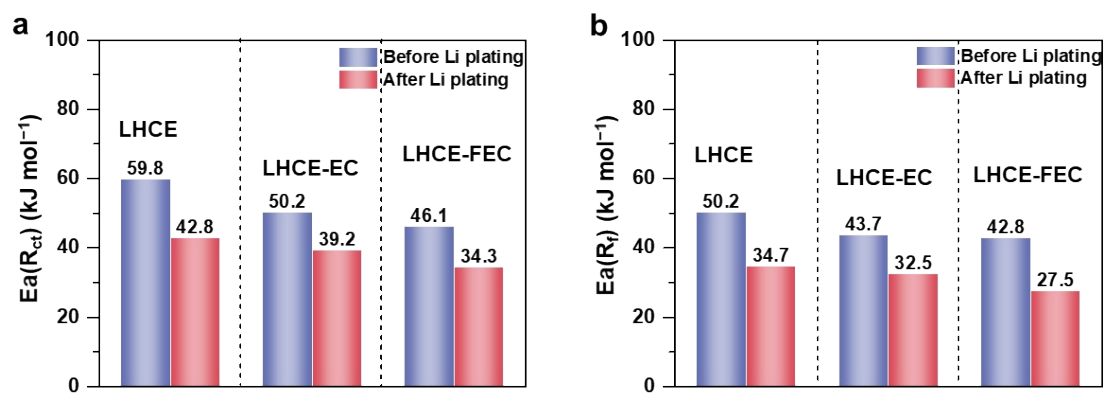
Figure S11. Activation energies derived from (a) the charge transfer impedance (R_{ct}) and (b) the interphase impedance (R_f) of anodes before and after Li plating using LHCE, LHCE-EC, and LHCE-FEC, respectively.
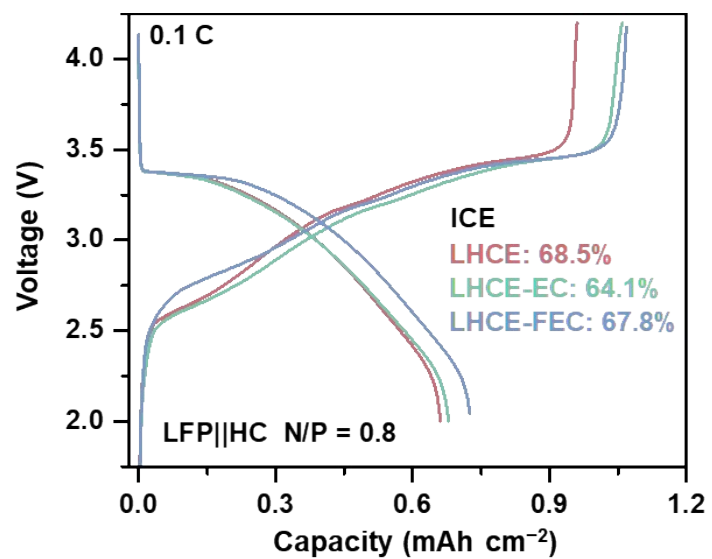
Figure S12. Voltage curves of the LFP||HC full cells using LHCE, LHCE-EC, and LHCE-FEC at the initial cycle under 0.1 C. Voltage range: 2.0~4.2 V.
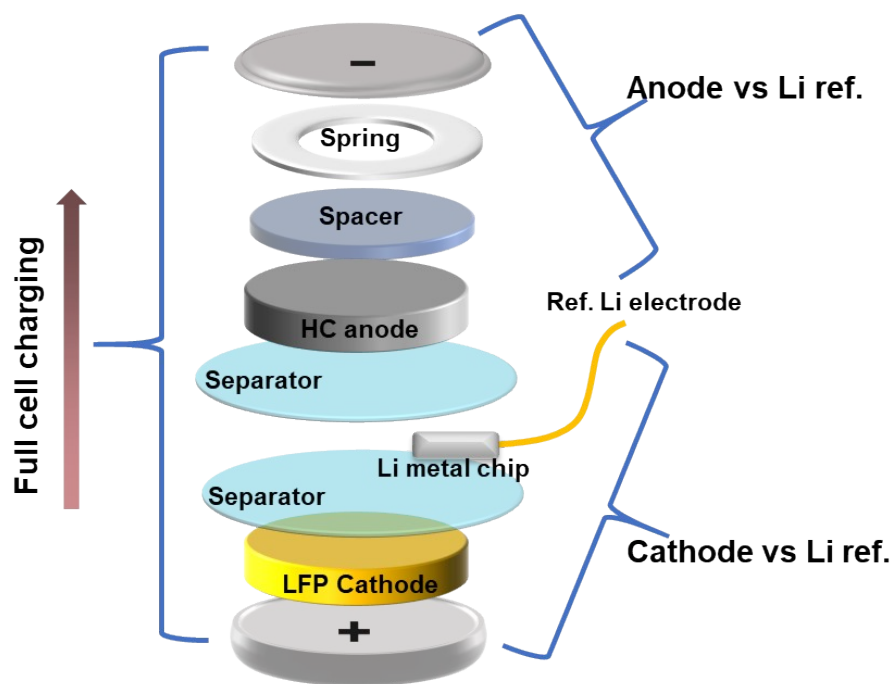
Figure S13. Schematic setup of the three-electrode cell assembly for Li plating measurements in LFP||HC full cells.
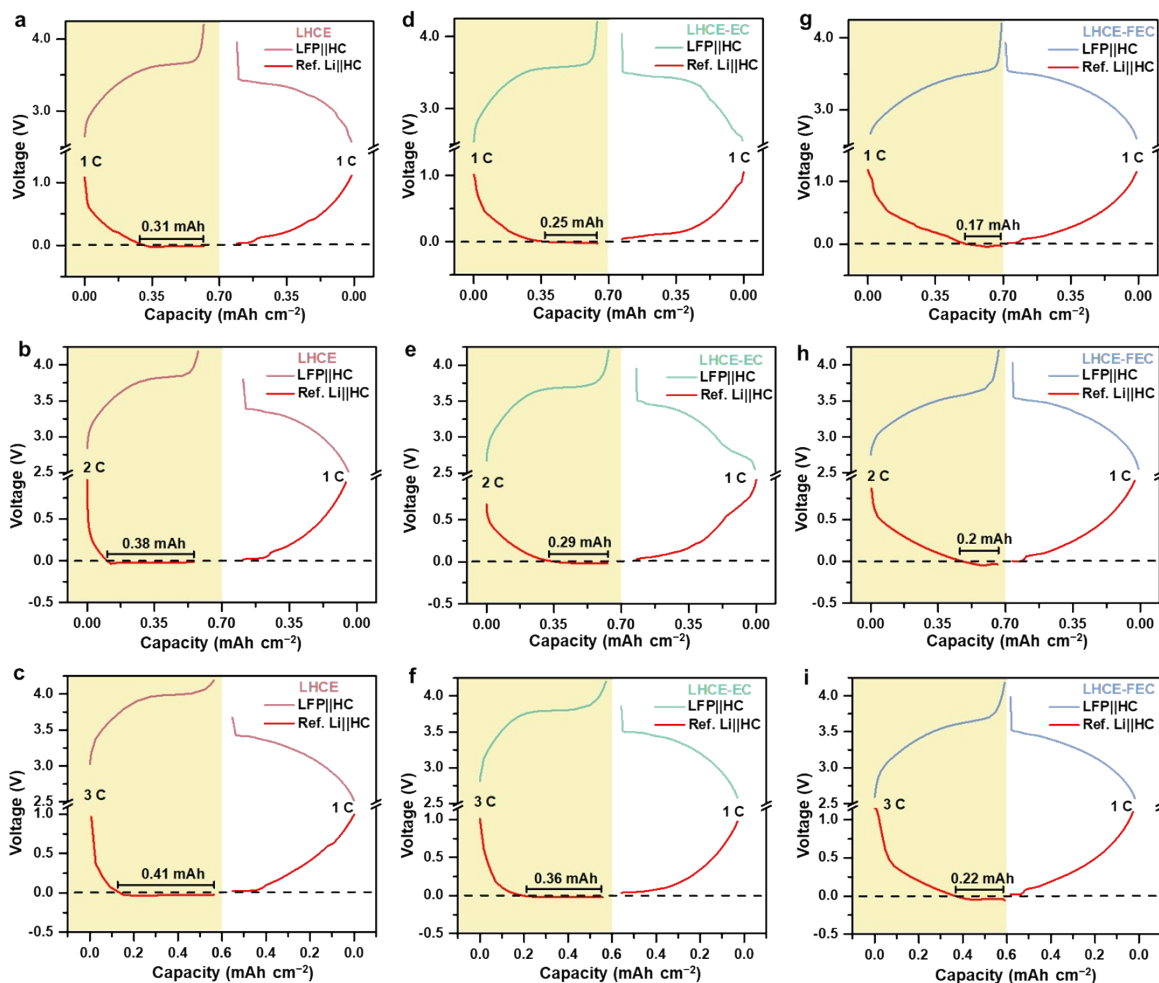
Figure S14. Voltage curves of three-electrode using Li metal as a reference electrode (Ref. Li) for LFP‖HC cells using LHCE at (a) 1 C, (b) 2 C, and (c) 3 C. Voltage curves of three-electrode using Li metal as a Ref. Li for LFP‖HC cells using LHCE-EC at (d) 1 C, (e) 2 C, and (f) 3 C. Voltage curves of three-electrode using Li metal as a Ref. Li for LFP‖HC cells using LHCE-FEC at (g) 1 C, (h) 2 C, and (i) 3 C. 1 C= 0.9 mAh cm^{-2}. Voltage range: 2.0~4.2 V.
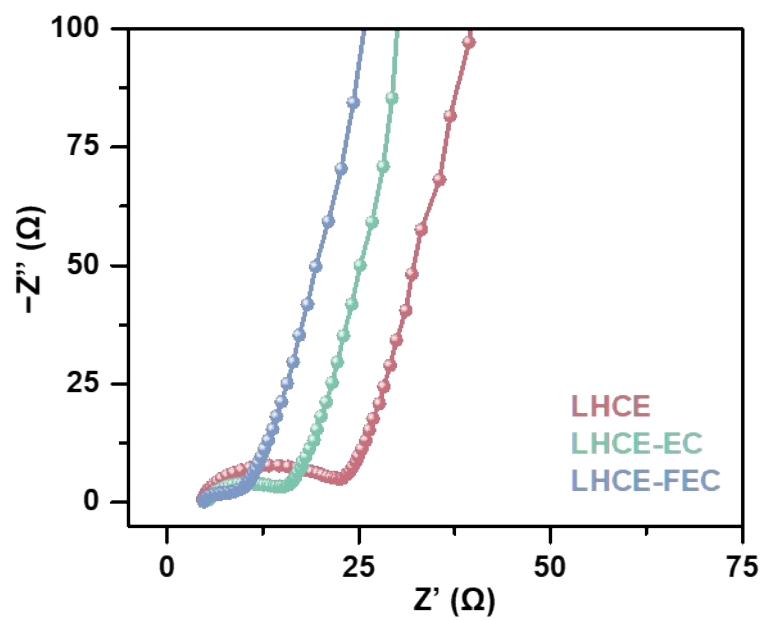
Figure S15. EIS spectra of the LFP||HC cell using LHCE, LHCE-EC, and LHCE-FEC before cycling.
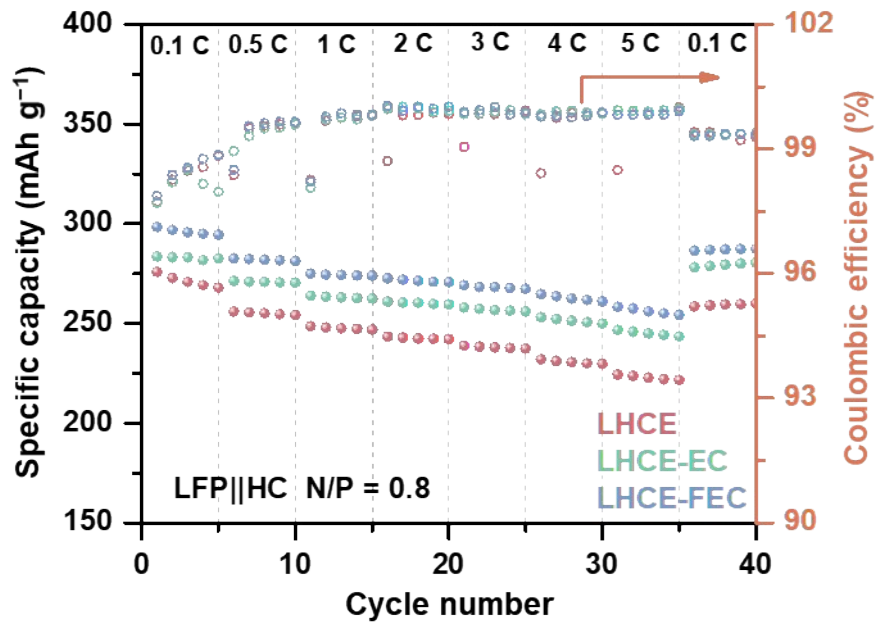
Figure S16. Rate performance of LFP||HC full cells using LHCE, LHCE-EC, and LHCE-FEC at 0.1~5 C. Voltage range: 2.0~4.2 V.
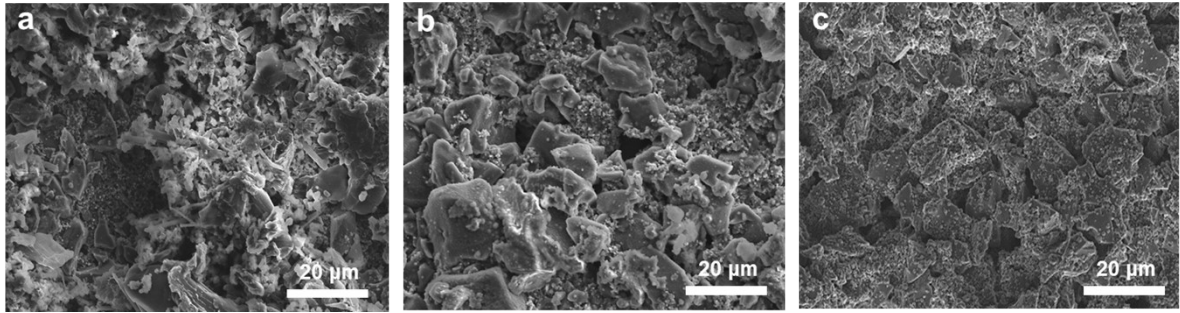
Figure S17. SEM images of HC anodes cycled in LFP‖HC full cells using (a) LHCE, (b) LHCE-EC, and (c) LHCE-FEC after 400 cycles at 1 C.
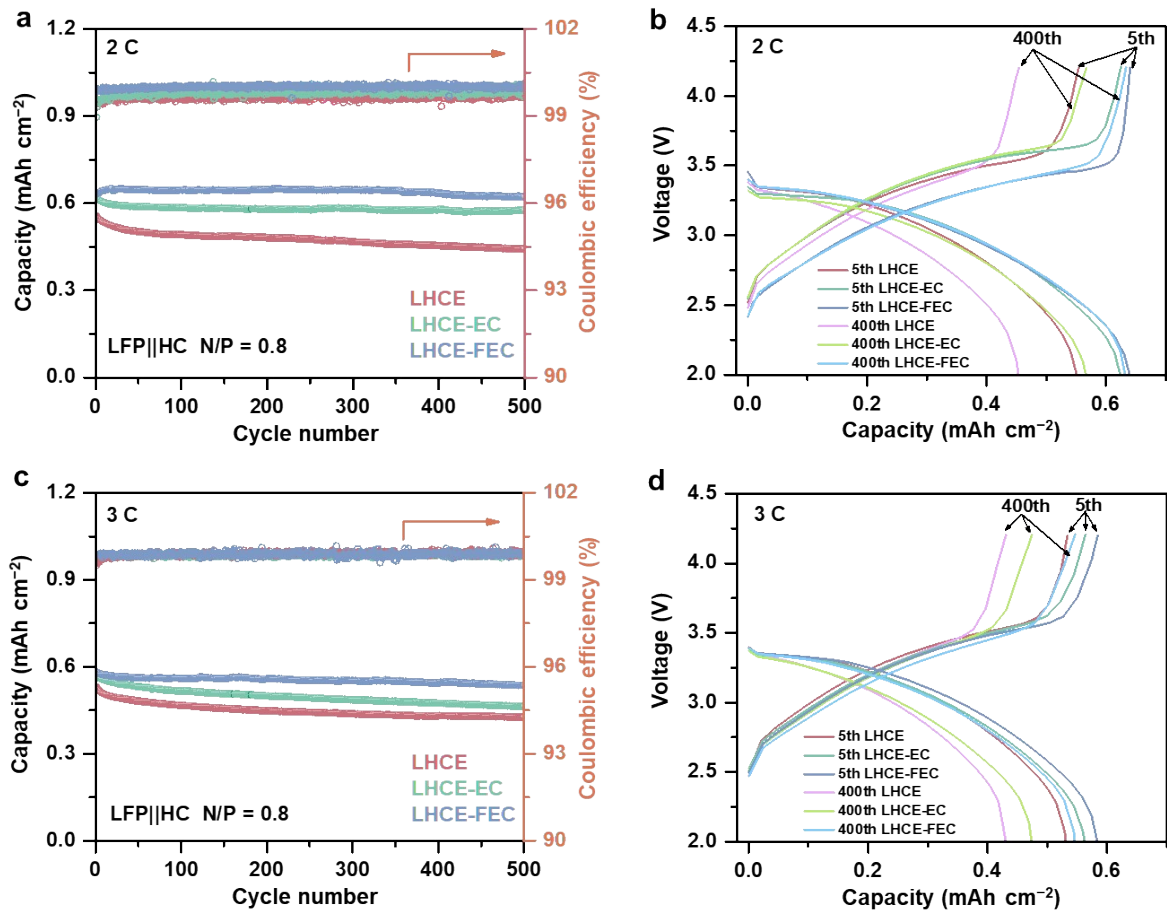
Figure S18. (a) Cycling performance and (b) voltage curves of LFP‖HC cells in LHCE, LHCE-EC, and LHCE-FEC at 2 C. (c) Cycling performance and (d) voltage curves of LFP‖HC cells in LHCE, LHCE-EC, and LHCE-FEC at 3 C. 1 C = 0.9 mAh cm^{-2}. Voltage range: 2.0~4.2 V.

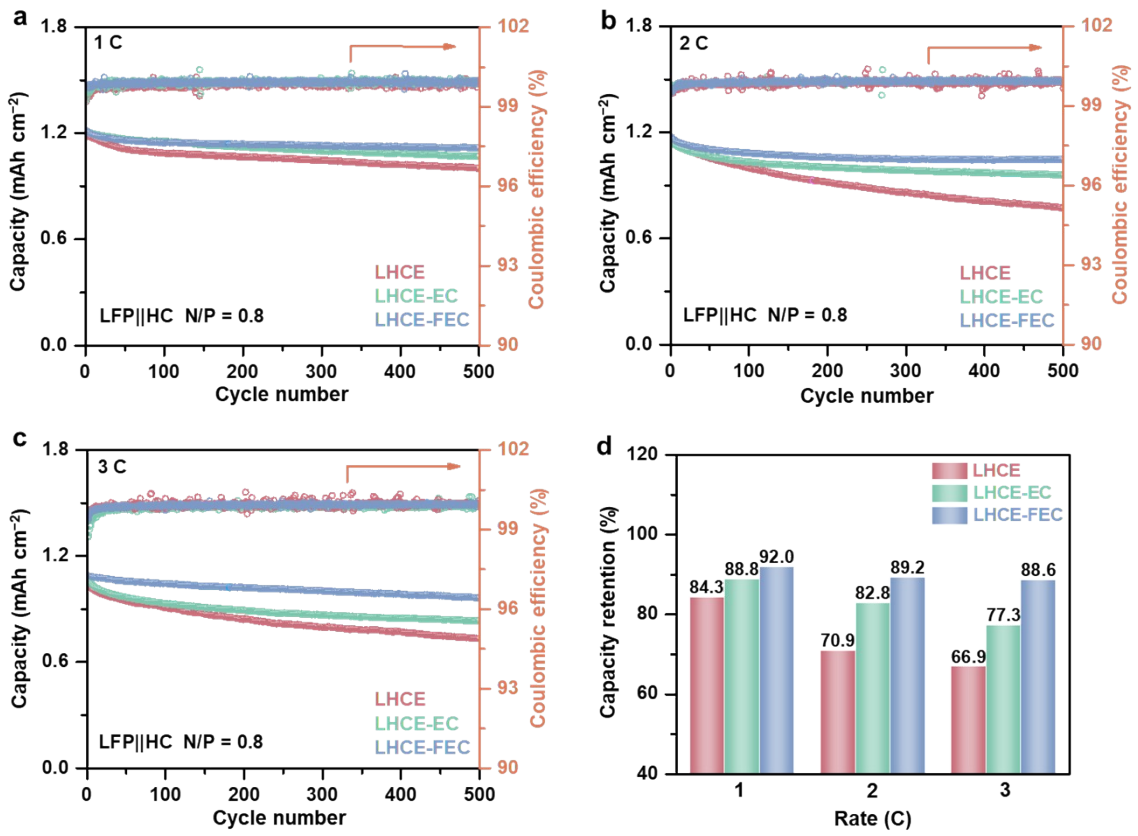Figure S19. Cycling performance of LFP‖HC cells using LHCE, LHCE-EC, and LHCE-FEC at (a) 1 C, (b) 2 C, and (c) 3 C. (d) Capacity retention of LFP‖HC cells using LHCE, LHCE-EC, and LHCE-FEC at 1~3 C after 500 cycles. 1 C = 1.5 mAh cm^{-2}. Voltage range: 2.0~4.2 V.
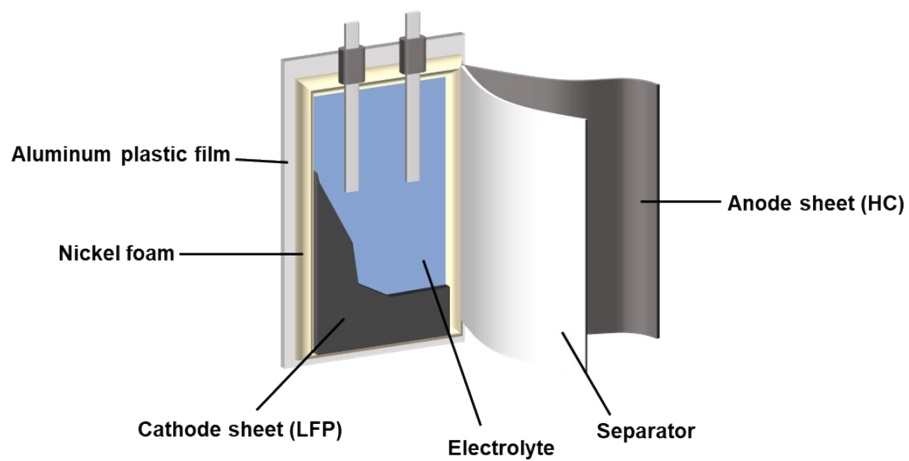
Figure S20. Schematic assembly of the single-layer LFP||HC pouch cell.
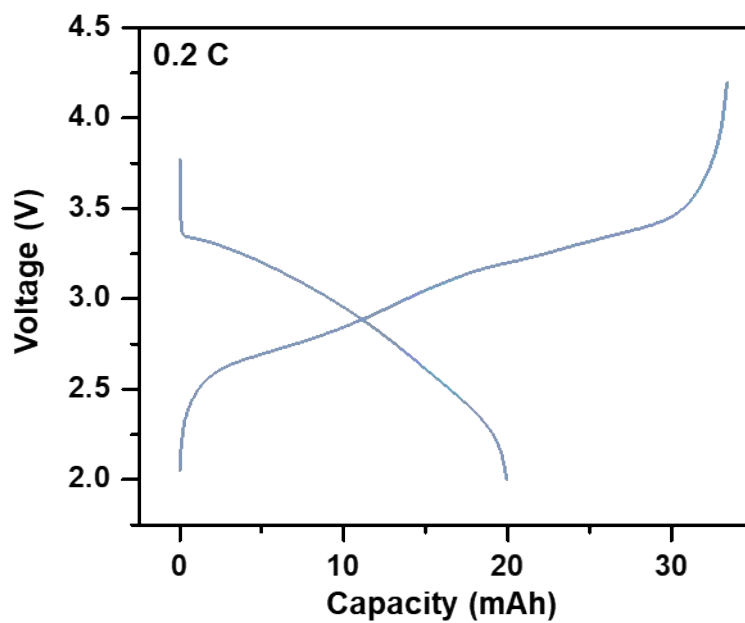
Figure S21. The initial voltage profiles of the pouch cell in LHCE-FEC at 0.2 C. 1 C = 20 mAh. Voltage range: 2.0~4.2 V.

Figure S22. Charging voltage profiles of 20-mAh LFP‖HC pouch cells using (a) CCE, (b) LHCE, (c) LHCE-EC, and (d) LHCE-FEC at 1~10 C. 1 C = 20 mAh. Voltage range: 2.0~4.2 V.
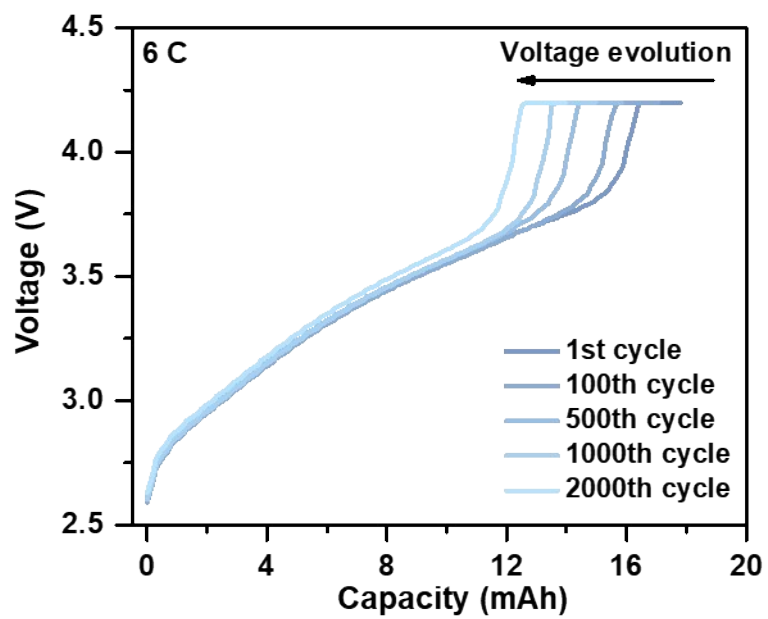
Figure S23. Charging voltage evolution of the pouch cell using LHCE-FEC at various cycles under 6-C cycling.
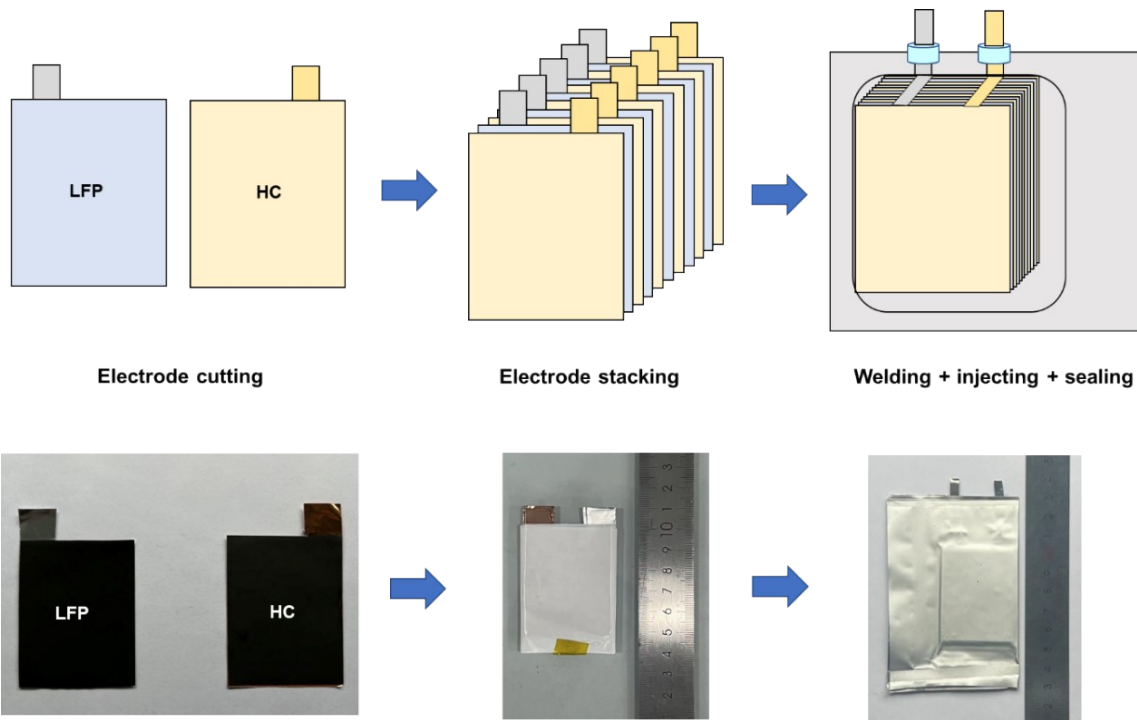
Figure S24. Illustration and preparation process of laminated double-side LFP cathode and HC anode sheets for 200-mAh LFP||HC pouch cells.
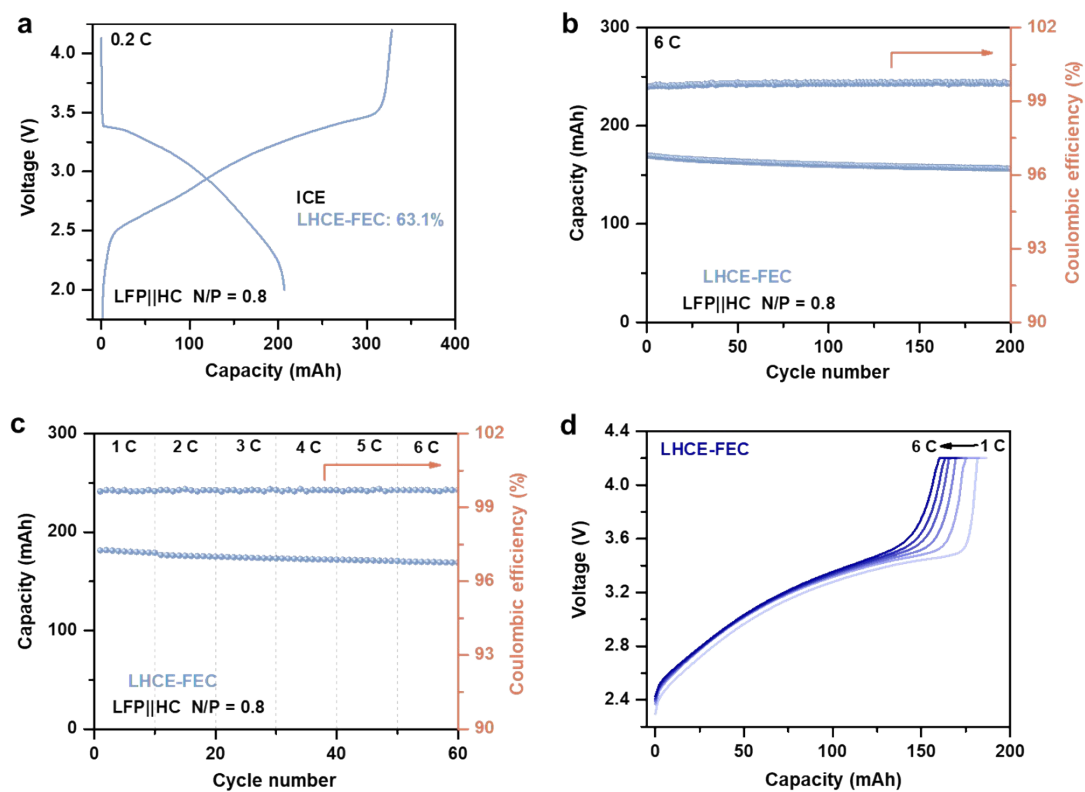
Figure S25. (a) The initial voltage profiles of the pouch cell using LHCE-FEC at 0.2 C. (b) Cycling performance of pouch c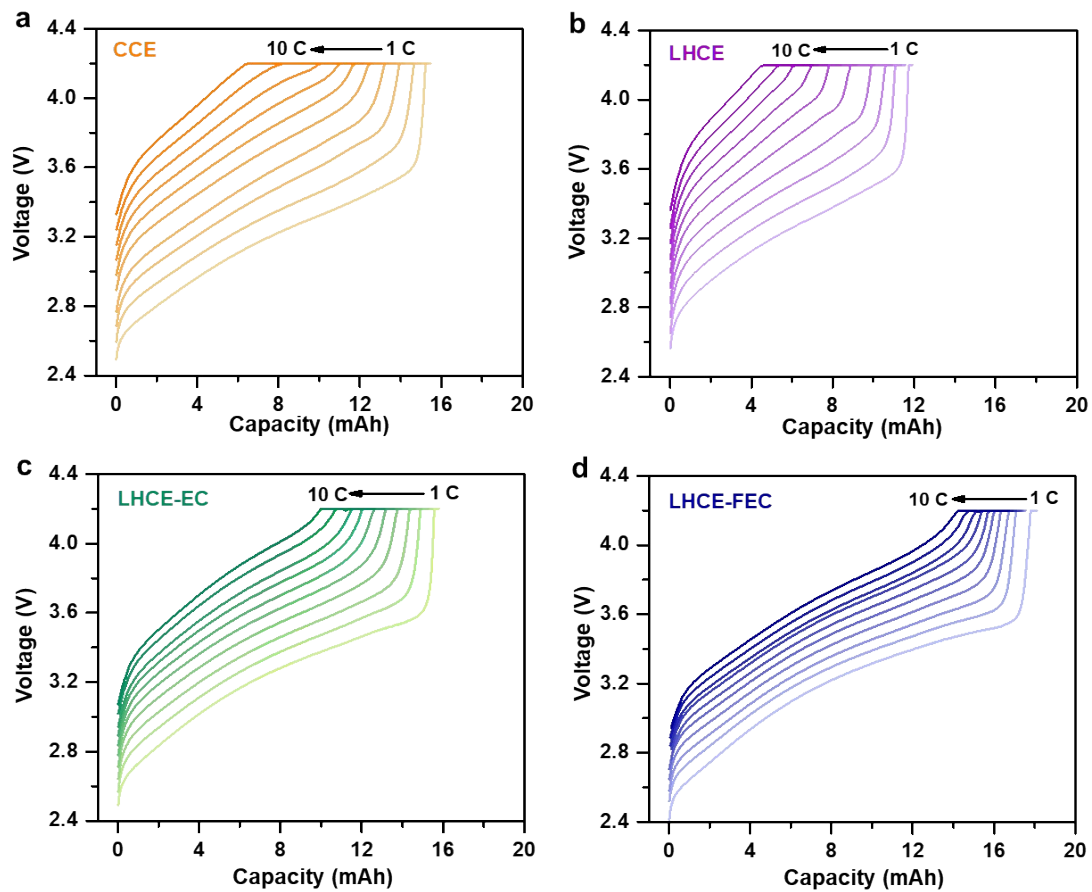ells using LHCE-FEC at 6 C. (c) Rate performance and (d) corresponding charging voltage profiles of 200-mAh LFP||HC pouch cells using LHCE-FEC at 1~6 C. 1 C = 200 mAh. Voltage range: 2.0~4.2 V.

Table S1. Li$^+$ transference numbers in various LHCEs calculated by the potentiostatic polarization method.

Electrolytes	Ro (Ω)	Rs (Ω)	Io (mA)	Is (mA)	ΔV (mV)	t_{Li}^+
LHCE	213.0	235.2	0.045	0.035	10	0.23
LHCE-EC	190.3	214.9	0.049	0.038	10	0.25
LHCE-FEC	141.1	183.4.4	0.073	0.042	10	0.30

Table S2. Calculated adsorption energies of FSI/EC/FEC in various adsorption configurations.

Species	Structure	Adsorption energy (eV)
Anion	FSI (w/o SV)	−2.60
	FSI (SV)	−2.48
Additive	EC	−1.01
	FEC	−0.92
Additive-anion	EC-FSI	−3.25
	FEC-FSI	−3.08
Li-additive-anion	Li-EC-FSI	−4.32
	Li-FEC-FSI	−3.97

Table S3. Pouch cell parameters.

20-mAh pouch cell	Specifications	Indications & Values
Cathode	Cathode material	LiFePO$_4$
	Cathode loading (mg cm^{-2})	12
	Active material fraction (%)	92%
	Al weight (mg cm^{-2})	4
	Compact density (g mL^{-1})	2.4
Anode	Anode material	Hard carbon
	Anode loading (mg cm^{-2})	4.5
	Active material fraction (%)	90%
	Cu weight (mg cm^{-2})	7.35
	Compact density (g mL^{-1})	1.4
Cell	Separator thickness (μm)	12
	Cell dimension (cm × cm)	4.1 × 5.1
	Electrolyte injection (mL)	1
	Nominal capacity (mAh)	33

Table S4. Summary of recent progress on carbonaceous anode under fast-charging conditions.

Electrolyte compositions	Cathode‖Anode	N/P ratio	Real capacity	Charging C-rate	CC-stage SOC	Ref.
1.4M LiFSI DMC/HFE/FEC (25:40:1 v/v/v)	LFP‖HC	0.8	0.02 Ah	6 C	82.2%	This work
1.4M LiFSI DMC/HFE/FEC (25:40:1 v/v/v)	LFP‖HC	0.8	0.2 Ah	6 C	80.6%	This work
1.6M LiFSI DMC/HFE/EC (30:40:1 v/v/v)	NMC532‖Gr	0.8	1.2 Ah	6 C	28.4%	32
1.0M $LiPF_6$ EC/DMC (3:7 v/v)	NMC622‖Gr	1.1	0.1 Ah	6 C	43%	55
1.0M LiTFSI + 0.5M $LiPF_6$ DMC/FEC (2:8 v/v)	NCA‖Gr	1.08	1 Ah	6 C	50.4%	53
1.0M $LiPF_6$ EC/DMC (1:1 v/v) + 5 vol.%FEC + 5 vol.% 4M $LiNO_3$ in triglyme	LFP‖Gr	0.8	1.2 Ah	6 C	51%	33
1.0M $LiPF_6$ EC/EMC (3:7 v/v) + 2 wt.%VC	NMC532‖HC	1.16	1.15 Ah	6 C	54.8%	54
1.0M $LiPF_6$ EC/EMC (3:7 v/v) + 2 wt.%VC	NMC532‖Gr/HC	1.16	1.26 Ah	6 C	65.1%	54
1.0M $LiPF_6$ EC/DMC/DEC/EP/PN (20:40:10:15:15 w/w/w/w/w) + 3 wt.%VC +3 wt.%FEC	NMC532‖Gr	1.12	0.03 Ah	6 C	67.7%	58
1.0M $LiPF_6$ EC/DMC (3:7 v/v)	NMC622‖P-S-Gr	1.1	0.1 Ah	6 C	72%	55
1.0M $LiPF_6$ EC/EMC (3:7 v/v) + 2 wt.%VC	NMC532‖Gr	1.16	1.3 Ah	6 C	72.3%	54
1.0M $LiPF_6$ EC/EMC (3:7 v/v) + 2 wt.%VC	NMC532‖HOLE Gr	1.1~1.2	2.2 Ah	6 C	76.4%	56
1.2M $LiPF_6$ EC/EMC (3:7 w/w)	NMC532‖Gr	1.17	0.019 Ah	6 C	77.3%	57

SI Reference

1. M. J. Frisch, G. W. Trucks, H. B. Schlegel, G. E. Scuseria, M. A. Robb, J. R. Cheeseman, G. Scalmani, V. Barone, G. A. Petersson, H. Nakatsuji, X. Li, M. Caricato, A. V. Marenich, J. Bloino, B. G. Janesko, R. Gomperts, B. Mennucci and D. J. Hratch, 2016, Gaussian 16, Revision C.01 Gaussian, Inc., Wallingford CT.

2. Y. L. Wang, F. U. Shah, S. Glavatskih and O. Antzutkin, A, *J. Phys. Chem. B,* 2014, **118**, 8711.

3. M. J. Abraham, T. Murtola, R. Schulz, S. Páll, J. C. Smith, B. Hess and E. Lindahl, *SoftwareX*, 2015, **1**, 19-25.

4. C. Z. Zhao, P. Y. Chen, R. Zhang, X. Chen, B. Q. Li, X. Q. Zhang, X. B. Cheng and Q. Zhang, *Sci. Adv.*, 2018, **4**, eaat3446.

5. Z. J. Cao, B. Li and S. B. Yang, *Adv. Mater.*, 2019, **31**, 1901310.

6. S. Y. Li, Q. L. Liu, J. J. Zhou, T. Pan, L. N. Gao, W. D. Zhang, L. Fan and Y. Y. Lu, *Adv. Funct. Mater.*, 2019, **29**, 1808847.

7. J. P. Perdew, K. Burke and M. Ernzerhof, *Phys. Rev. Lett.*, 1996, **77**, 3865.

8. X. L. Li, J. Bao, Y. F. Li, D. Chen, C. Ma, Q. Q. Qiu, X. Y. Yue, Q. C. Wang and Y. N. Zhou, *Adv. Sci.* 2021, **8**, 2004448.

9. G. Kresse and J. Hafner, *Phys. Rev. B*, 1993, **47**, 558.

10. P. E. Blöchl, *Phys. Rev. B*, 1994, **50**, 17953.

11. J. Klimeš, D. R. Bowler and A. Michaelides, *J. Phys. Condens. Matter*, 2010, **22**, 022201.